

Demonstration of a Corner-cube-interferometer LWIR Hyperspectral Imager

Ingmar G. E. Renhorn · Thomas Svensson ·
Staffan Cronström · Tomas Hallberg · Rolf Persson ·
Roland Lindell · Glenn D. Boreman

Received: 15 June 2009 / Accepted: 14 July 2009 /
Published online: 25 July 2009
© Springer Science + Business Media, LLC 2009

Abstract An interferometric long-wavelength infrared (LWIR) hyperspectral imager is demonstrated, based on a Michelson corner-cube interferometer. This class of system is inherently mechanically robust, and should have advantages over Sagnac-interferometer systems in terms of relaxed beamsplitter-coating specifications, and wider unvignetted field of view. Preliminary performance data from the laboratory prototype system are provided regarding imaging, spectral resolution, and fidelity of acquired spectra.

Keywords Hyperspectral Imaging · LWIR · Corner-cube Interferometer

1 Introduction

There is a continuing interest in interferometric hyperspectral imagers using infrared focal plane array (FPA) sensors. Different configurations are possible, scanning the interferometer mirror to produce high-resolution spectra for each pixel of a static scene [1, 2], or scanning the image in one dimension through a static interferogram. Generally, the image scan motion uses the pushbroom geometry, with one dimension of scanning accomplished by the movement of the optics platform. The rows and columns of the FPA data produce snapshots of the scene as it scans in the horizontal direction. Each row of FPA data has an interferogram associated with it for each scan position. The scene moves relative to the static interferogram and successive interferograms represent sequential pixels of a given row. Given the advantage of a mechanically robust optical train, the Sagnac interferometer is an often-used configuration, with a number of successfully fielded instruments [3–6].

However, one optical path in the Sagnac transits the beamsplitter twice in transmission, while the other path is reflected twice from the beamsplitter. Because of this, the Sagnac

I. G. E. Renhorn · T. Svensson · S. Cronström · T. Hallberg · R. Persson · R. Lindell
FOI — Swedish Defense Research Agency, P.O. Box 1165, SE-581 11 Linköping, Sweden

G. D. Boreman (✉)
University of Central Florida, CREOL/College of Optics & Photonics, Orlando, FL 32816-2700, USA
e-mail: boreman@creol.ucf.edu

design is known to suffer a loss in beamsplitter efficiency when the reflection and transmission are not 50% over the wavelength range of the instrument. Compared to a Michelson configuration where the beamsplitter is traversed once in transmission and once in reflection, this directly reduces the fringe contrast in the interferogram, and hence the signal-to-noise ratio (SNR) as function of wavelength. Beamsplitter efficiencies for Michelson and Sagnac static-interferometer configurations are compared in [7].

Also, because of its relatively long optical path, the field of view (FOV) of a Sagnac imaging interferometer is limited by vignetting, with the beamsplitter being the limiting element. Interferometric imagers based on a Michelson configuration, but using two-dimensional dihedral mirrors, have been shown [8] to have better vignetting performance, with the limiting dimension being the aperture of the dihedral mirrors. A comparison of vignetting effects for Michelson and Sagnac interferometers is seen in [9]. Corner-cube Michelson interferometers have been investigated in various contexts [10–13], with their appeal stemming from the angular insensitivity of the corner cubes resulting in relaxed alignment tolerances.

Motivated primarily by the desire to relax the beamsplitter-coating specifications, and with the expectation that a corner-cube design would ultimately yield a mechanically robust and easy-to-align instrument with a relatively wide FOV, we present the first, to our knowledge, demonstration of a laboratory prototype hyperspectral imager based on a Michelson corner-cube configuration. The instrument operates with an uncooled bolometric focal plane in the LWIR 8–14 μm band. We provide demonstration of imaging capability, with different interferogram/image regions acquired in different sections of the vertical FOV. Interferogram data are processed to produce spectral transmittance plots for thin samples of vinyl and polypropylene, with good agreement to spectral features of the samples measured with a laboratory spectrometer. Spectral resolution of the instrument is about 30 cm^{-1} FWHM.

2 Prototype instrument

The laboratory setup was based on a standard Michelson interferometer, but with the substitution of two front-surface (Au coated) corner-cube reflectors, of 63.5-mm diameter, purchased from Edmund Scientific. Specified retroreflection parallelism was 1 second of arc. The beamsplitter and a nominally identical compensator plate, purchased from II–VI Infrared, were made from ZnSe, in rectangular format 70 mm \times 100 mm \times 7 mm. One surface of the beamsplitter was a nominal 50/50 LWIR beamsplitter coating, while the other surface (and those of the compensator) were coated with a broadband antireflector, with less than 1% reflection across the 8–14 μm band. The two ZnSe plates were mounted together, separated by metallic shims of about 0.25-mm thickness, with the beamsplitter coating on an interior surface. It was found that the compensator plate was critical in obtaining high-contrast fringes from the thermal source. The path lengths of the two arms of the interferometer were measured with mechanical calipers, and adjusted as closely as possible to be equal. At this point, small longitudinal motions of one corner cube were sufficient to obtain white-light fringes. Compared to the zero-fringe condition, a relative horizontal position offset between the corner cubes on the order of 0.75 mm was introduced to produce a suitable linear fringe pattern with vertical orientation.

The IR camera was a Miricle 307 K, by Thermoteknix. Its bolometric focal plane was uncooled, in a 640 \times 480 format, with 25 μm pixel spacing in each direction. The f/1 camera

lens was Ge, with a 50-mm focal length, which was focused at infinity. With this lens, the nominal noise-equivalent temperature difference was 85 mK. The total dynamic range for output data was 14 bits. The objects used were freestanding films of vinyl and polypropylene, backlit by a 100°C extended-area blackbody source (SR-80 from CI Systems) of (10 cm)² area. With this setup, useful interference fringes were obtained nearly to the edge of the FOV. For the imaging demonstration, a Ge meniscus singlet lens (not optimized for image quality or vignetting), with $f \approx 50$ mm was placed between the interferometer and the object plane, to bring the object plane from its nominal infinity position into a convenient laboratory distance.

3 Data processing

Data records were typically obtained as 100 frame sequences, taken in 1/30 sec intervals. The individual frames of data in these sequences are averaged together to increase the SNR. Data is acquired from the focal plane for the case of both interferometer arms open, and for each arm blocked at the aperture of the corner cube. For the case where a single interferogram covers the whole FOV, the interferogram data set is divided by the average of the data sets for each arm blocked. This flat-fielding operation removes most vignetting-induced shading in the interferogram. A 100-line section at the center of the interferogram is averaged over the lines. The residual shading in the interferogram is removed by fitting the 640-pixel data set to a 6th-order polynomial, and dividing the data set by that polynomial. Unity is subtracted from the result, to get a zero mean function. A Hamming window is applied to the whole length of the data set, and the power spectrum is calculated. All of these operations are performed for both the blackbody and for the blackbody backlighting the plastic film. The spectrum of the blackbody plus film is divided by the spectrum of the blackbody to yield the transmittance spectrum of the film. The horizontal axis of this spectrum is proportional to wavenumber, and the vertical axis is proportional to transmittance. For each axis, a uniform scale factor is applied to obtain coincidence of major features of the independently-measured film transmittance with those of the data set. The independent transmittance measurements were performed on a Bruker IFS 55 spectrometer, with a spectral resolution of 0.24 cm⁻¹. To approximately match the resolution of the prototype instrument, the spectra from the Bruker were convolved with a triangular function with a FWHM of 30 cm⁻¹.

4 Measured data

In Fig. 1(a) and (b), we compare the transmittance spectra for the vinyl film and for the polypropylene film respectively. In each figure, the dotted line is the spectrum measured with the Bruker spectrometer, and the solid line is the spectrum measured with the corner-cube interferometer. In both cases, the agreement is quite good for the location and relative magnitude of the spectral features.

In Fig. 2(a), the interferogram for the vinyl film is presented. In this plot, the position numbers along the horizontal axis refer to the column number of the FPA. Data for all 640 columns of the FPA are shown, and it can be seen that useful interference fringes extend nearly to the edges of the instrument FOV. About 30 fringes are discernable above the noise level, and given a nominal wavelength of 10 μm, this agrees well with the noted spectral

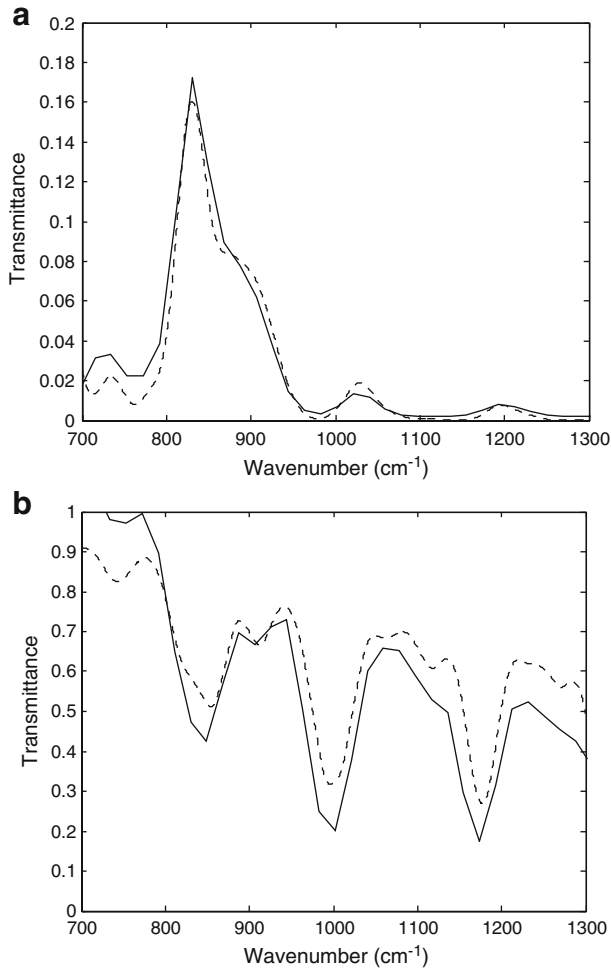


Fig. 1 Comparison of transmittance spectra, as measured by the Bruker spectrometer (dotted line) and the corner-cube interferometer (solid line). **(a)** Vinyl film. **(b)** Polypropylene film.

resolution of 30 cm^{-1} for the instrument. In Fig. 2(b), a full-FOV image is shown of an edge of the polypropylene film, showing details of an embossed structure. Two different interferograms are seen in the image, representing the film backlit by the 100°C blackbody, and the blackbody itself. It should be noted that the lens used to form the image was a simple Ge meniscus singlet lens, which was not optimized for either image-quality or vignetting performance.

5 Discussion

It can be seen that the position and relative magnitude of the spectral features of the plastic films measured by the corner-cube interferometer correspond well to spectra measured using the Bruker spectrometer. In the object-at-infinity configuration, interferogram data of

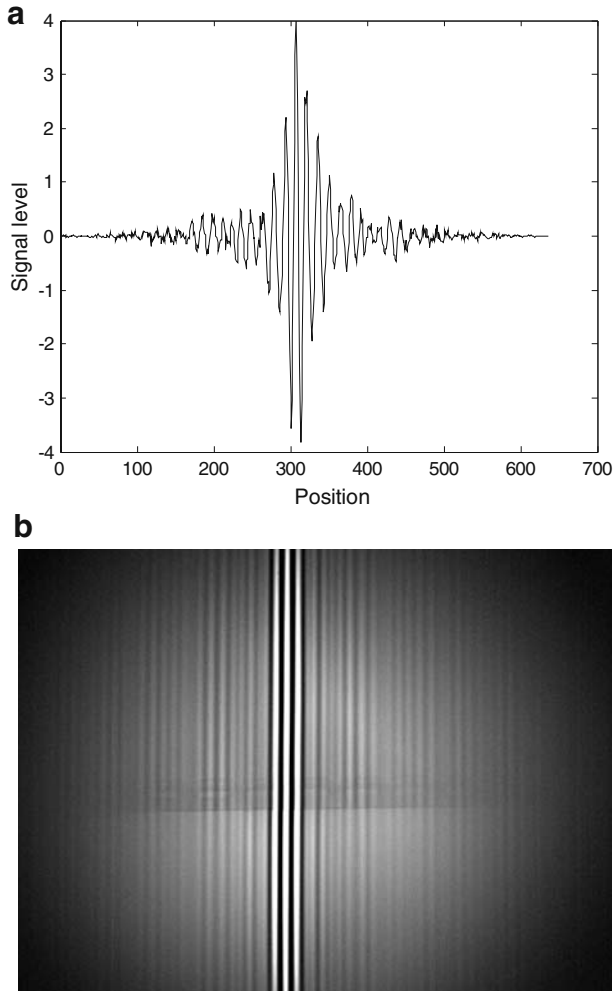


Fig. 2 (a) Interferogram of vinyl film. Horizontal axis is FPA column number, all 640 are shown. (b) Full-FOV image showing edge of polypropylene film backlit by 100°C blackbody.

useful SNR is obtained nearly to the edges of the FOV, which indicates a potential vignetting advantage of the corner-cube interferometer design. Imaging of a nearby object was accomplished using a simple lens in front of the interferometer, which was otherwise focused at infinity. If imaging of nearby objects were routinely desired, a more complex lens assembly would be needed, specifically corrected for image quality and vignetting. The corner-cube Michelson design is inherently robust mechanically, given that the relative alignment of the cubes is not sensitive to angle. Cost advantages may be seen compared to Sagnac designs, since because of the symmetric optical paths in the beamsplitter, fringe contrast is not significantly degraded by unequal reflection and transmission of the beamsplitter coating. The basic corner-cube interferometer design may well represent a viable path forward for stationary interferometric imagers used employed in a pushbroom-scan context, using both cooled and uncooled FPAs.

References

1. J. Giroux, J. Legault, Y. Montembeault, T. Smithson, A. Villemaire, and J. Arduin, Proc. SPIE **4719**, 144 (2002).
2. M. Chamberland, V. Farley, P. Lagueux, A. Villemaire, P. Dubois, and J. Gagnon, in *Fourier Transform Spectroscopy*, OSA Technical Digest, paper FThA2 (2009).
3. J. Rafert, R. Sellar, and J. Blatt, Appl. Opt. **34**, 7228 (1995).
4. P. Lucey and B. Wilcox, Proc. SPIE **5159**, 275 (2003).
5. P. Lucey, K. Horton, and T. Williams, Proc. SPIE **6546**, 65604 (2007).
6. P. Lucey, K. Horton, and T. Williams, Appl. Opt. **47**, F107 (2008).
7. P. Griffiths and J. De Haseth, *Fourier Transform Infrared Spectrometry*, 2nd edn. (Wiley, Hoboken, 2007), pp. 128–137.
8. Y. Ferrec, J. Taboury, H. Sauer, and P. Chavel, Opt. Eng. **45**, 115601 (2006).
9. R. Sellar and G. Boreman, Opt. Eng. **42**, 3320 (1995).
10. E. Peck, J. Opt. Soc. Am. **38**, 66 (1948).
11. E. Peck, J. Opt. Soc. Am. **38**, 1015 (1948).
12. M. Murty, J. Opt. Soc. Am. **50**, 7 (1960).
13. J. Kauppinen and P. Saarinen, Appl. Opt. **31**, 69 (1992).